

Uncertainty and Irreproducibility of Triboelectricity Based on Interface Mechanochemistry

Giulio Fatti¹, Hyunseung Kim,^{2,3} Changwan Sohn,^{2,3} Minah Park², Yeong-won Lim,^{2,3} Zhuohan Li⁴, Kwi-il Park⁵, Izabela Szlufarska⁶, Hyunseok Ko¹, Chang Kyu Jeong^{1,2,3,7,*}, and Sung Beom Cho^{1,8,9,†}

¹Center of Materials Digitalization, Korea Institute of Ceramic Engineering and Technology (KICET), Jinju, Gyeongsangnam-do 52851, Republic of Korea

²Division of Advanced Materials Engineering, Jeonbuk National University, Jeonju, Jeonbuk 54896, Republic of Korea

³Department of Energy Storage/Conversion Engineering of Graduate School and Hydrogen and Fuel Cell Research Center, Jeonbuk National University, Jeonju, Jeonbuk 54896, Republic of Korea

⁴Materials Science Division, Lawrence Berkeley National Laboratory, Berkeley, California 94720, USA

⁵School of Materials Science and Engineering, Kyungpook National University, Daegu 41566, Republic of Korea

⁶Department of Materials Science and Engineering, University of Wisconsin-Madison, Madison, Wisconsin 53706-1595, USA

⁷Department of JBU-KIST Industry-Academia Convergence Research, Jeonbuk National University, Jeonju, Jeonbuk 54896, Republic of Korea

⁸Department of Materials Science and Engineering, Ajou University, Suwon, Gyeonggi-do 16499, Republic of Korea

⁹Department of Energy Systems Research, Ajou University, Suwon, Gyeonggi-do 16499, Republic of Korea

(Received 18 November 2022; revised 22 May 2023; accepted 15 September 2023; published 19 October 2023)

Triboelectrification mechanism is still not understood, despite centuries of investigations. Here, we propose a model showing that mechanochemistry is key to elucidate triboelectrification fundamental properties. Studying contact between gold and silicate glasses, we observe that the experimental triboelectric output is subject to large variations and polarity inversions. First principles analysis shows that electronic transfer is activated by mechanochemistry and the tribopolarity is determined by the termination exposed to contact, depending on the material composition, which can result in different charging at the macroscale. The electron transfer mechanism is driven by the interface barrier dynamics, regulated by mechanical forces. The model provides a unified framework to explain several experimental observations, including the systematic variations in the triboelectric output and the mixed positive-negative “mosaic” charging patterns, and paves the way to the theoretical prediction of the triboelectric properties.

DOI: 10.1103/PhysRevLett.131.166201

Triboelectrification (TE), the transfer of electrostatic charges between two materials in contact, is one of the longest studied physical problems. Despite being investigated since the eighteenth century [1,2], very little conclusive understanding has been achieved on its underlying mechanism. For a long time, scientists believed that materials had an inherent tendency to charge more or less positively or negatively, and they devised the so-called triboelectric series to order materials according to their triboelectric charging [3–5]. However, several experimental observations conflict with the very idea of such ordering. Triboelectric series have proved uncertain and hard to reproduce [6]. Distinct samples of the same materials can change their positions on the triboelectric series, and triboelectric charging can change even on the same sample after consecutive experiments [5–10]. For instance, glasses and silicates are a major example of this irreproducibility, as they systematically show different charging in different experiments [4,5,11–14].

The reasons for this systematic irreproducibility have not been fully understood to date. In general, different charge carriers may govern the physics of TE, electrons [15–18],

ions [19–21], and tiny fragments of material transferred in the contact [22–24]. Theoretical models have mostly focused on electron transfer, especially after recent experimental findings suggested that solid-solid TE is mainly caused by electrons [16,17]. For example, the surface state model [25,26], the effective work function model [27–29], and the interface potential barrier model [30] have been proposed to explain electron-driven TE. However, these models often fail to reproduce the experimental observations. The more recent backflow-stuck charges (BSC) model proposed a more successful explanation [31], establishing a positive correlation between electron-driven triboelectric charging and the electrostatic potential barrier existing at the contact interface. A schematic defining the electrostatic barrier is shown in the Supplemental Material (SM), Note S1 [32]. According to the model, electron transfer is caused by mechanical forces upon contact, but some charges flow back to their original material through tunneling. Hence, only electrons remaining stuck after transfer contribute to TE. A higher electrostatic barrier thus prevents larger electron backflow and results in a higher TE. The BSC model has been able to capture some features of metal-dielectric

TE, successfully describing the triboelectric series of tribopositive oxides.

However, even the most refined models based only on electron transfer cannot grasp the full complexity of the experimental measurements. First, in the tribology community it is universally accepted that mechanochemical reactions are ubiquitous in frictional contact, causing bond ruptures and ionic transfer [65–71]. Second, atomic force microscopy measurements have shown that nanoscale charging is always found in a mosaic of both positive and negative charged regions. Therefore, the net macroscopic charge is given by the balance between these mixed island of positive and negative charges [33,72]. These measurements have been reproduced several times [73–75], showing that this feature is universal and might be inherently related to ion transfer [22], whose mechanism has not been described yet.

In this letter, combining experimental measurements and first principles calculations, we demonstrate that mechanochemistry and ion transfer are indeed key to trigger electron-driven TE. We analyzed a selected set of gold-silicates pairs, chosen for their especially unclear triboelectric behavior, and confirmed the inherent irreproducibility of the measurements, applying a statistical approach. To elucidate the underlying mechanism, we employed first principles calculations to devise the first theoretical mechanochemistry-based model of TE, generalizing the BSC model to include ionic transfer. The model shows that (i) mechanochemistry can be crucial to prompt electron-driven TE, and that (ii) tribopolarity is determined by the chemical properties of the surface terminations exposed by mechanochemistry, implying that only certain materials can switch polarity depending on their surface terminations' chemical composition. Additionally, we tested our model on TiO_2 , corroborating our results. Importantly, the model does not involve ions as charge carriers, but highlights how mechanochemical ion transfer can enable electron transfer. Hence, the model can be coherently combined with other recent models involving flexoelectricity and thermoelectricity [76–79]. Our findings explain a broad range of experimental observations, from the mosaic charge patterns to the irreproducible triboelectric series, including them in a unified theoretical framework.

Figure 1 shows our triboelectric measurements for the selected materials, namely quartz, fused silica, and borosilicate glass. The choice of these materials allows us to evaluate the contribution to TE played by chemical composition and crystallinity. Figure 1(a) schematically represents the triboelectric generator employed for the measurements. Triboelectric generators can be designed in different operation modes that can collect tribocharges either by sliding or by vertical contact-separation (CS) motion [80]. We employed a CS configuration, schematically depicted in Fig. 1(a), to exclude complications arising from sliding motion, such as shear effects, for a better

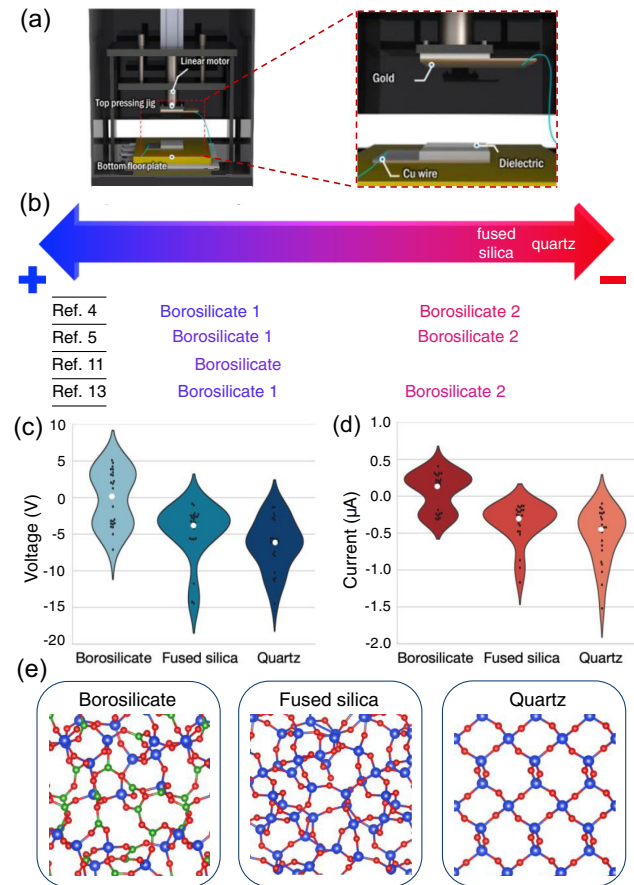


FIG. 1. Triboelectrification experimental measurements of silica and borosilicate glass. (a) Schematics of the experimental apparatus for the vertical CS mode. (b) Qualitative triboelectric series extracted from references [4,5,11,13]. (c),(d) Violin plots showing, respectively, the highly variable distribution of the measured voltages and currents. (e) Snapshots of the borosilicate, fused silica, and quartz structures as employed for the density-functional theory calculations. Blue: Si, Red: O, Green: B.

comparison with theoretical calculations. Contact with gold, chemically inert and triboelectrically neutral, guarantees a reliable evaluation of the triboelectric output. Further details are provided in the Methods 1 section of the SM.

According to previous reports [4,5,11–14], while fused and quartz silica occupy well-defined positions on the triboelectric series, borosilicate glass can switch polarity. Figure 1(b) shows a qualitative comparison between previously reported series. Our measurement distributions show that the actual triboelectric signal can significantly vary at every measurement, spanning a wide range of voltages and currents, respectively displayed in the violin plots in Figs. 1(c) and 1(d). For all three types of material, the distributions have long tails deviating from the bulk of the distribution, which demonstrates a wide uncertainty of the results. However, both fused silica and quartz reveal a steadily negative triboelectric charging and a similar

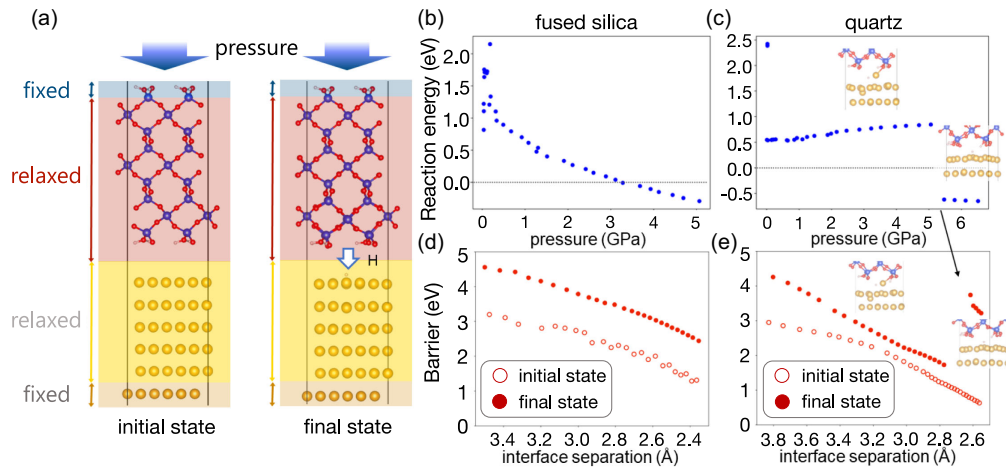


FIG. 2. Effect of indentation on reaction energy and electrostatic barrier. (a) Silica on gold indentation is modeled *ab initio* simulating the initial (before mechanochemistry) and the final state (after) at a fixed interface distance, and then progressively reducing this distance to increase the pressure quasistatically. (b),(d) Reaction energy at every indentation step, respectively, for fused silica and quartz. (c),(e) Interface barrier before (unfilled circles) and after (filled circles) hydrogen transfer, respectively, for fused silica and quartz.

distribution, while borosilicate shows a bimodal distribution, with two distinct peaks with opposite polarities. A complete list of references is in the SM, Note S2 [32]. Since the measurement distributions can be multimodal, like for borosilicate, the triboelectric series cannot be defined using the distribution average. This would fail to capture the triboelectric behavior, as it would predict an almost neutral output, instead of a triboelectric charge fluctuating between negative and positive. This is highlighted by the white dots representing the average of the distributions in Figs. 1(b) and 1(c).

To understand the systematic uncertainty observed in the measurements, we investigated nanoscale contact by means of first principles calculations. The employed structures are shown in Fig. 1(e) and described accurately in the SM, Methods 3. First, we tested the BSC model, investigating the triboelectric behavior of the hydroxylated surfaces of the selected materials [34,81,82], involving only electron transfer [32]. Analyzing the partial charges by means of Bader analysis, we found a negligible triboelectric charging of 10^{-2} e and, coherently with the BSC model [31], a very low barrier at the gold-silicate interface. However, as this clearly contradicts the experimental measurements, electron transfer alone cannot explain TE, meaning that transfer of chemical species must be involved.

Therefore, we modeled silicate-gold contact under pressure to study the activation of hydrogen transfer by mechanical forces and to evaluate the effect on TE of the newly formed dangling bond. We applied a methodology first introduced to describe mechanochemical reactions from first principles [35]. In this method, the effect of pressure on chemistry is investigated by applying a quasistatic indentation of the silicates against gold. As shown in Fig. 2(a), we started from a fixed interface separation and relaxed the configuration before (initial

configuration) and after (final configuration) ionic transfer. Using the calculated energies, we computed the reaction energy as $E_r = E_{\text{final}} - E_{\text{initial}}$. After relaxation we moved the silicate closer to the gold, relaxed again both the initial and the final configuration, re-computed the reaction energy, and iterated the process. More details on the procedure can be found in the SM, Note S5 [32]. Figures 2(b) and 2(c) show the reaction energy E_r against the applied pressure for the hydrogen transfer from fused silica and quartz, respectively. The reaction becomes energetically favorable at very high pressures, in the order of the GPa, 4 orders of magnitude larger than the nominal experimental pressure of 10^5 Pa . However, it is known that nominally flat surfaces are comprised of multiple nanoasperities [83] and the local pressure on single asperities can be up to 10^5 times higher than the macroscopic pressure applied experimentally, as shown in the SM, Fig. S6 [32,36,37,84–87]. The calculated pressure range is indeed consistent with previous measurements of single asperity contact [88]. In a real-life situation, flash temperatures and kinetic effects should contribute to further reducing the pressure needed to activate the mechanochemical reaction [89]. It should be noted that gold deforms plastically, which is in agreement with previous reports where it has been observed even to a very large extent [38].

Figures 2(d) and 2(e) show the evolution of the interface barrier as the indentation proceeds, before (unfilled circles) and after (filled circles) hydrogen transfer. Two major points emerge from these results. First, the barrier rises significantly after the mechanochemical reaction. This immediately points out to an increase in the triboelectric charging, according to the BSC model. Electronic transfer is indeed confirmed by calculations performed at the equilibrium. Note S7 in the SM shows that different

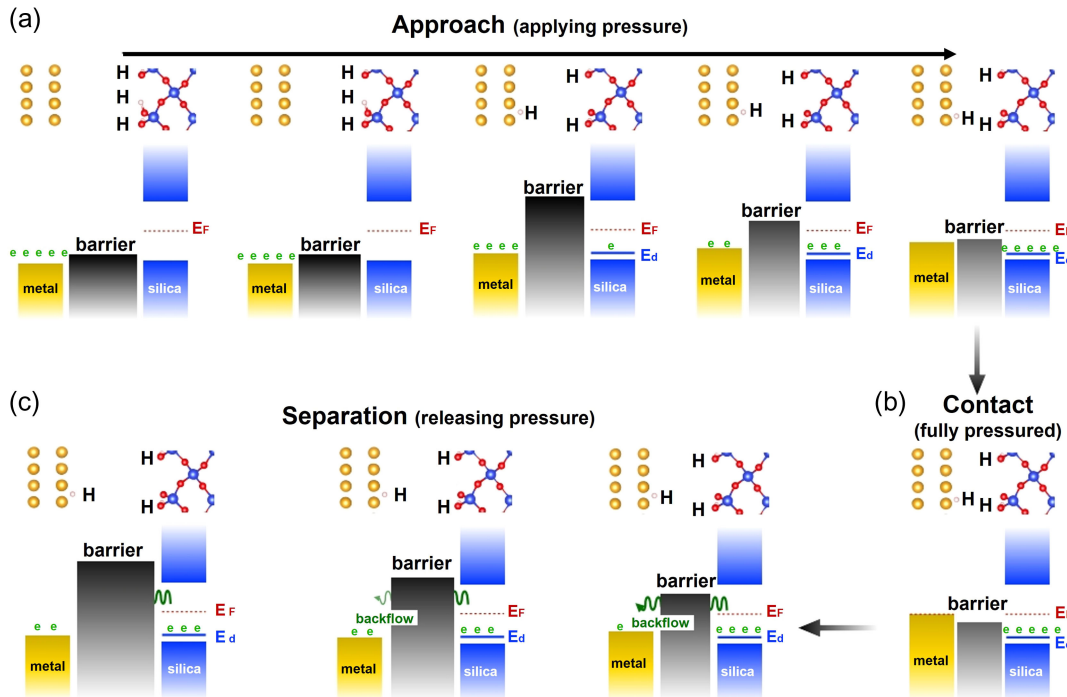


FIG. 3. Mechanism of triboelectrification due to mechanochemical ion transfer. (a) In the approaching stage initially triboelectrification is prevented by the absence of dangling bonds. As the pressure increases, mechanochemical ion transfer is activated and charge transfer begins (forward flow). The increasing pressure lowers the interface barrier and favors a larger charge transfer. (b) At full contact the maximum amount of charge is transferred. (c) During separation a fraction of the transferred charges flows back to gold, tunneling the barrier (backflow), until it becomes too high to be tunneled.

terminations exposed by mechanochemical reactions acquire a large charge, demonstrating that TE is enabled by mechanochemistry. This charge is fully electronic, with no ionic contribution, as shown in the SM, Note S8 [32]. Moreover, we find that the calculated electrostatic barrier and triboelectric charging are proportional, further corroborating the BSC model. Secondly, as silica and gold are pressed against each other, the interfacial barrier reduces by as much as 50%. This barrier drop is significant because it facilitates electron transfer, as we have shown with a numerical simulation of the tunneling probability across the quantum barrier in the SM, Note S9. Experimentally, kinetic effects due to the nonequilibrium nature of contact, not present in the simulations, are likely to further contribute to the transfer [90]. Based on this consideration, we propose a mechanism to include mechanochemistry in the description of the microscopic TE process.

Figure 3 shows the scheme of our proposed model. We conceptually schematize the contact in three stages: approach, full contact, and separation. In the approaching stage [Fig. 3(a)] the silicate gets closer to gold under the effect of external mechanical stresses. Initially, pressure is low, and no chemical reaction occurs. Since the barrier is low, any transferred charge is free to flow back to the more stable state on its original material. This stage corresponds to the unfilled dots in Figs. 2(d) and 2(e). As indentation proceeds, mechanical stresses activate mechanochemical

reactions. This generates dangling bonds on the silicate surface that allow electronic transfer, resulting in a sudden barrier hike [the filled dots in Figs. 2(d) and 2(e)], in agreement with the BSC model. Under increasing pressure, interface separation continues to narrow, lowering again the barrier and enabling additional charge transfer—the forward flow. This process shows that TE is indeed activated by mechanical stresses, an assumption of the BSC model that is demonstrated here.

At full contact stage [Fig. 3(b)], triboelectric charging reaches its maximum value. First, the Fermi levels of gold and the silicate in contact are aligned, implying that the highest-occupied states in gold are energetically unfavorable with respect to defect states in the silicate, inducing a flow of electrons toward the more stable states.

During separation [Fig. 3(c)] the excess charges captured by the silicate start to experience a drive to flow back to their original state due to the relief of pressure and the inversion of the kinetic motion. As pressure is relieved, electron backflow is activated by tunneling or lattice vibrations [31]. Backflow is stronger when the barrier is still low but, with increasing separation, the barrier progressively raises and the backflow slows down until it eventually stops, as shown in the last step, Fig. 3(c). The height of the barrier governs how quickly the backflow completely stops and determines the final quantity of stuck charges. The mechanism here proposed improves and generalizes the BSC model to a much wider class of

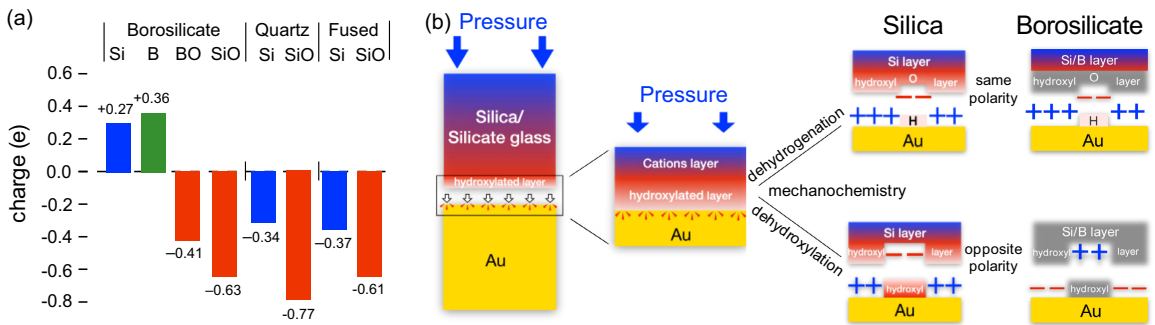
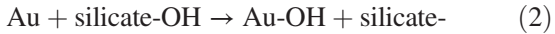


FIG. 4. Tribopolarity connected to different terminations. (a) Triboelectrification of the possible terminations, respectively, for borosilicate, quartz, and fused silica, expressed in elementary charge units e . (b) Schematics of the tribopolarity mechanism. Mechanochemical bonds rupture prompt charge transfer on the exposed anions or cations. These charge negatively in pure silica, while borosilicate cations charge positively.

situations, describing the effect of mechanochemistry on TE in metal-dielectric contact.

Once we explained the mechanochemical process, we investigated the influence of different terminations on tribopolarity. We considered two possible mechanochemical reactions leading to ionic transfer and to the exposure of dangling bonds to contact:



Reaction (1) breaks the O–H bond and exposes the oxygen anion to contact. Reaction (2) severs the bond between oxygen and the cation, leaving a dangling bond on silicon in fused silica and quartz, and on silicon or boron in borosilicate. Figure 4(a) shows the possible terminations for each considered material and their calculated triboelectric charging at the equilibrium interface distance. Borosilicate has four possible terminations (Si $-$, B $-$, SiO $-$, and BO $-$), while fused silica and quartz have only Si $-$ and SiO $-$. In both fused silica and quartz the calculated triboelectric charging is negative for each termination, consistent with previous studies performed by means of high-accuracy first principles investigations [91–93], supported by experimental evidence [94,95]. These reports have demonstrated that both SiO $-$ and Si $-$ surface defects act as deep electron traps, consistent with our finding that both terminations contribute to negative TE. Borosilicate can instead switch tribopolarity depending on the termination. As shown in Fig. 4(a), cationic Si $-$ and B $-$ acquire positive tribocharge, while the anionic SiO $-$ and BO $-$ charge negatively.

Figure 4(b) shows a schematic of the mechanism leading to different TE observed between pure silica and borosilicate. This can be related to their different chemical composition. In pure silica, both anionic (O $-$) and cationic (Si $-$) terminations contribute to negative triboelectric charging, while in borosilicate they switch polarity. This suggests an explanation for the high variability observed in

the experiments. Experimentally, the macroscopic TE output will be determined by the charge balance induced by the occurrence of multiple mechanochemical reactions. Several anionic and cationic terminations will be exposed, each contributing to triboelectric charging. The effect of plastic deformation will then promote the local convergence of positive or negative terminations, forming separate positive and negative areas [33,39]. This arrangement breaks the equiprobability between asperities of opposite polarities, leading to a non-neutral macroscopic charging, depending on the details and history of contact and on the environmental conditions (SM, Note S10). Thus, borosilicate charging can oscillate between tribopositivity and tribonegativity, depending on whether positive or negative areas come to be dominant at the interface. On the other hand, because silica terminations are always tribonegative, its macroscopic TE output will always be negative, even though it can change in magnitude with the number of actual mechanochemical events. In this case, the different number of mechanochemical events occurring at every measurement can also explain the distribution of the silica triboelectric output, as more reactions induce a larger charging and vice versa. Finally, borosilicate samples often contain concentrations of sodium oxide (Na₂O) that can contribute to TE, as shown in the SM, Note S11 [96]. The mechanism is corroborated by the results on the additional test material TiO₂, shown in Note S12.

In conclusion, we have proposed a mechanochemical model for TE to explain the systematic uncertainty observed in the experimental measurements. By investigating the contact between selected silicates and gold as a notable case study, we have shown that electronic transfer is enabled by the mechanochemical reactions occurring at the nanoasperities in contact. We have further generalized the BSC model, showing that the dynamics of electronic transfer is regulated by the variation of the interface barrier in the contact-separation motion. Through the model we have demonstrated that the tribopolarity of a material is determined by what terminations are exposed to contact. For example, cationic terminations are tribonegative in pure

silica but tribopositive in borosilicate. The macroscopic triboelectric output will be then governed by the surface balance between the positive and negative terminations. These findings explain several experimental observations, from the uncertain triboelectric output to the mosaic charging patterns, unifying them in a comprehensive theoretical framework. Moreover, our model is complementary to other models that have recently tried to explain TE based on the high stresses at the nanoasperity contact, highlighting the role of flexoelectricity or thermoelectricity [75–78]. Relating TE to the chemical properties of the species composing a material, we pave the way for the theoretical prediction of TE.

We gratefully acknowledge the support from the National Research Foundation of Korea funded by the Korean government (2022R1A2C4002037, 2022R1A4A3032923, RS-2023-00209910, and 2022-R1F1A1093060). The computations were carried out using resources from Korea Supercomputing Centers (KSC-2023-CRE-0348). Z. L. and I. S. gratefully acknowledge support from the US National Science Foundation Grant No. GEO-1951314.

- [11] H. Zuo, L. Guo, H. Xue, Y. Zhang, X. Shen, X. Liu, P. Wang, X. He, G. Dai, P. Jiang, H. Zheng, B. Zhang, C. Xu, and Z. L. Wang, Quantifying and understanding the triboelectric series of inorganic non-metallic materials, *Nat. Commun.* **11**, 1 (2020).
- [12] D. Ferguson, A basic triboelectric series for heavy minerals from inductive electrostatic separation behaviour, *J. South Afr. Inst. Min. Metall.* **110**, 75 (2010).
- [13] G. Freeman and N. March, Triboelectricity and some associated phenomena, *Mater. Sci. Technol.* **15**, 1454 (1999).
- [14] J. Henniker, Triboelectricity in polymers, *Nature (London)* **196**, 474 (1962).
- [15] Z. L. Wang and A. C. Wang, On the origin of contact-electrification, *Mater. Today* **30**, 34 (2019).
- [16] C. Xu, Y. Zi, A. C. Wang, H. Zou, Y. Dai, X. He, P. Wang, Y.-C. Wang, P. Feng, D. Li, and Z. L. Wang, On the electron-transfer mechanism in the contact-electrification effect, *Adv. Mater.* **30**, 1706790 (2018).
- [17] S. Lin, L. Xu, C. Xu, X. Chen, A. C. Wang, B. Zhang, P. Lin, Y. Yang, H. Zhao, and Z. L. Wang, Electron transfer in nanoscale contact electrification: Effect of temperature in the metal–dielectric case, *Adv. Mater.* **31**, 1808197 (2019).
- [18] S. Park, J. Park, Y.-g. Kim, S. Bae, T.-W. Kim, K.-I. Park, B. H. Hong, C. K. Jeong, and S.-K. Lee, Laser-directed synthesis of strain-induced crumpled MoS₂ structure for enhanced triboelectrification toward haptic sensors, *Nano Energy* **78**, 105266 (2020).
- [19] A. F. Diaz, D. Wollmann, and D. Dreblow, Contact electrification: Ion transfer to metals and polymers, *Chem. Mater.* **3**, 997 (1991).
- [20] L. S. McCarty and G. M. Whitesides, Electrostatic charging due to separation of ions at interfaces: Contact electrification of ionic electrets, *Angew. Chem. Int. Ed.* **47**, 2188 (2008).
- [21] L. S. McCarty, A. Winkleman, and G. M. Whitesides, Ionic electrets: Electrostatic charging of surfaces by transferring mobile ions upon contact, *J. Am. Chem. Soc.* **129**, 4075 (2007).
- [22] H. T. Baytekin, B. Baytekin, J. T. Incorvati, and B. A. Grzybowski, Material transfer and polarity reversal in contact charging, *Angew. Chem. Int. Ed.* **51**, 4843 (2012).
- [23] A. Ciniero, G. Fatti, M. C. Righi, D. Dini, and T. Reddyhoff, A combined experimental and theoretical study on the mechanisms behind tribocharging phenomenon and the influence of triboemission, *Tribol. Online* **14**, 2019 (2019).
- [24] L. Lapčinskis, A. Linarts, K. Mālnieks, H. Kim, K. Rubenis, K. Pudzs, K. Smits, A. Kovalčovs, K. Kalniņš, A. Tamm, C. K. Jeong, and A. Šutka, Triboelectrification of nanocomposites using identical polymer matrixes with different concentrations of nanoparticle fillers, *J. Mater. Chem. A* **9**, 8984 (2021).
- [25] D. J. Lacks, N. Duff, and S. K. Kumar, Nonequilibrium Accumulation of Surface Species and Triboelectric Charging in Single Component Particulate Systems, *Phys. Rev. Lett.* **100**, 188305 (2008).
- [26] L. Ernst, Optical spectroscopy of surface states on NaCl and KCl crystals and its relation to contact charging, *Solid State Commun.* **19**, 515 (1976).
- [27] F.-C. Chiu, A review on conduction mechanisms in dielectric films, *Adv. Mater. Sci. Eng.* **2014**, 578168 (2014).

- [28] A. Franciosi and C. G. Van de Walle, Heterojunction band offset engineering, *Surf. Sci. Rep.* **25**, 1 (1996).
- [29] Z. Zhong and P. Hansmann, Band Alignment and Charge Transfer in Complex Oxide Interfaces, *Phys. Rev. X* **7**, 011023 (2017).
- [30] J. Wu, X. Wang, H. W. Li, Feng, W. Yang, and Y. Hu, Insights into the mechanism of metal-polymer contact electrification for triboelectric nanogenerator via first-principles investigations, *Nano Energy* **48**, 607 (2018).
- [31] H. Ko, Y.-w. Lim, S. Han, C. K. Jeong, and S. B. Cho, Triboelectrification: Backflow and stuck charges are key, *ACS Energy Lett.* **6**, 2792 (2021).
- [32] See Supplemental Material at <http://link.aps.org/supplemental/10.1103/PhysRevLett.131.166201> for more details, which includes Refs. [5,11,22,31,33–64].
- [33] H. Baytekin, A. Patashinski, M. Branicki, B. Baytekin, S. Soh, and B. Grzybowski, The mosaic of surface charge in contact electrification, *Science* **333**, 302 (2011).
- [34] A. Rimola, D. Costa, M. Sodupe, J.-F. Lambert, and P. Ugliengo, Silica surface features and their role in the adsorption of biomolecules: Computational modeling and experiments, *Chem. Rev.* **113**, 4216 (2013).
- [35] Z. Li and I. Szlufarska, Physical Origin of the Mechanochemical Coupling at Interfaces, *Phys. Rev. Lett.* **126**, 076001 (2021).
- [36] T. D. Jacobs and A. Martini, Measuring and understanding contact area at the nanoscale: A review, *Appl. Mech. Rev.* **69**, 060802 (2017).
- [37] V. A. Yastrebov, G. Anciaux, and J.-F. Molinari, From infinitesimal to full contact between rough surfaces: Evolution of the contact area, *Int. J. Solids Struct.* **52**, 83 (2015).
- [38] L.-F. Wang, Y. Dong, M.-H. Hu, J. Tao, J. Li, and Z.-D. Dai, Evolution of surfaces and mechanisms of contact electrification between metals and polymers, *Chin. Phys. B* **31**, 066202 (2022).
- [39] O. Verners, L. Lapčinskis, L. Germane, A. Kasikov, M. Timusk, K. Pudzs, A. V. Ellis, P. C. Sherrell, and A. Šutka, Smooth polymers charge negatively: Controlling contact electrification polarity in polymers, *Nano Energy* **104**, 107914 (2022).
- [40] G. Kresse and J. Furthmüller, Efficiency of ab-initio total energy calculations for metals and semiconductors using a plane-wave basis set, *Comput. Mater. Sci.* **6**, 15 (1996).
- [41] J. P. Perdew, K. Burke, and M. Ernzerhof, Generalized Gradient Approximation Made Simple, *Phys. Rev. Lett.* **77**, 3865 (1996).
- [42] G. Kresse and D. Joubert, From ultrasoft pseudopotentials to the projector augmented-wave method, *Phys. Rev. B* **59**, 1758 (1999).
- [43] P. E. Blöchl, Projector augmented-wave method, *Phys. Rev. B* **50**, 17953 (1994).
- [44] A. Jain, S. P. Ong, G. Hautier, W. Chen, W. D. Richards, S. Dacek, S. Cholia, D. Gunter, D. Skinner, G. Ceder, and K. A. Persson, Commentary: The materials project: A materials genome approach to accelerating materials innovation, *APL Mater.* **1**, 011002 (2013).
- [45] S. P. Ong, W. D. Richards, A. Jain, G. Hautier, M. Kocher, S. Cholia, D. Gunter, V. L. Chevrier, K. A. Persson, and G. Ceder, Python materials genomics (pymatgen): A robust, open-source python library for materials analysis, *Comput. Mater. Sci.* **68**, 314 (2013).
- [46] A. Pedone, G. Malavasi, M. C. Menziani, U. Segre, and A. N. Cormack, Molecular dynamics studies of stress-strain behavior of silica glass under a tensile load, *Chem. Mater.* **20**, 4356 (2008).
- [47] D. J. Evans and B. L. Holian, The nose-hoover thermostat, *J. Chem. Phys.* **83**, 4069 (1985).
- [48] W. Tang, E. Sanville, and G. Henkelman, A grid-based Bader analysis algorithm without lattice bias, *J. Phys. Condens. Matter* **21**, 084204 (2009).
- [49] E. Sanville, S. D. Kenny, R. Smith, and G. Henkelman, Improved grid-based algorithm for Bader charge allocation, *J. Comput. Chem.* **28**, 899 (2007).
- [50] M. Yu and D. R. Trinkle, Accurate and efficient algorithm for Bader charge integration, *J. Chem. Phys.* **134**, 064111 (2011), [10.1063/1.3553716](https://doi.org/10.1063/1.3553716).
- [51] M. L. Hair, Hydroxyl groups on silica surface, *J. Non-Cryst. Solids* **19**, 299 (1975).
- [52] A. S. D’Souza and C. G. Pantano, Mechanisms for silanol formation on amorphous silica fracture surfaces, *J. Am. Ceram. Soc.* **82**, 1289 (1999).
- [53] W. A. Adeagbo, N. L. Doltsinis, K. Klevakina, and J. Renner, Transport processes at α -Quartz–water interfaces: Insights from first-principles molecular dynamics simulations, *ChemPhysChem* **9**, 994 (2008).
- [54] Á. Cimas, F. Tielens, M. Sulpizi, M. P. Gaigeot, and D. Costa, The amorphous silica–liquid water interface studied by *ab initio* molecular dynamics (AIMD): Local organization in global disorder, *J. Phys. Condens. Matter* **26**, 244106 (2014).
- [55] A. Rimola, D. Costa, M. Sodupe, J. F. Lambert, and P. Ugliengo, Silica surface features and their role in the adsorption of biomolecules: Computational modeling and experiments, *Chem. Rev.* **113**, 4216 (2013).
- [56] L. T. Zhuravlev and V. V. Potapov, Density of silanol groups on the surface of silica precipitated from a hydrothermal solution, *Russ. J. Phys. Chem.* **80**, 1119 (2006).
- [57] L. T. Zhuravlev, The surface chemistry of amorphous silica. Zhuravlev model, *Colloids Surf. A* **173**, 1 (2000).
- [58] T. M. Mayer, J. E. Houston, G. E. Franklin, A. A. Erchak, and T. A. Michalske, Electric field induced surface modification of Au, *J. Appl. Phys.* **85**, 8170 (1999).
- [59] COMSOL Multiphysics, Introduction to COMSOL multiphysics®, COMSOL Multiphysics, Burlington, MA, accessed Feb 9(2018), 32 (1998).
- [60] O. Verners, L. Lapčinskis, L. Germane, A. Kasikov, M. Timusk, K. Pudzs, A. V. Ellis, P. C. Sherrell, and A. Šutka, Smooth polymers charge negatively: Controlling contact electrification polarity in polymers, *Nano Energy* **104**, 107914 (2022).
- [61] D. G. Jeong, Y. J. Ko, J. H. Kim, D. S. Kong, Y. C. Hu, D. W. Lee, S. H. Im, J. Lee, M. S. Kim, G.-H. Lee, C. W. Ahn, J. R. Ahn, M. Lee, J. Y. Park, and J. H. Jung, On the origin of enhanced power output in ferroelectric polymer-based triboelectric nanogenerators: Role of dipole charge versus piezoelectric charge, *Nano Energy* **103**, 107806 (2022).
- [62] M. Rarivomanantsoa, P. Jund, and R. Jullien, Sodium diffusion through amorphous silica surfaces: A molecular dynamics study, *J. Chem. Phys.* **120**, 4915 (2004).

- [63] N. V. Tran, A. K. Tieu, H. Zhu, H. T. Ta, P. T. Sang, H. M. Le, and T. D. Ta, Insights into the tribochemistry of sliding iron oxide surfaces lubricated by sodium silicate glasses: An *ab initio* molecular dynamics study, *Appl. Surf. Sci.* **528**, 147008 (2020).
- [64] M. Ren, L. Deng, and J. Du, Bulk, surface structures and properties of sodium borosilicate and boroaluminosilicate nuclear waste glasses from molecular dynamics simulations, *J. Non-Cryst. Solids* **476**, 87 (2017).
- [65] F. Galembeck, T. Burgo, L. Balestrin, R. Gouveia, C. Silva, and A. Galembeck, Friction, tribochemistry and triboelectricity: Recent progress and perspectives, *RSC Adv.* **4**, 64280 (2014).
- [66] A. L. Barnette, D. B. Asay, D. Kim, B. D. Guyer, H. Lim, M. J. Janik, and S. H. Kim, Experimental and density functional theory study of the tribochemical wear behavior of SiO_2 in humid and alcohol vapor environments, *Langmuir* **25**, 13052 (2009).
- [67] H. He, L. Qian, C. G. Pantano, and S. H. Kim, Effects of humidity and counter-surface on tribochemical wear of soda-lime-silica glass, *Wear* **342–343**, 100 (2015).
- [68] M. Wang, F. Duan, and X. Mu, Effect of surface silanol groups on friction and wear between amorphous silica surfaces, *Langmuir* **35**, 5463 (2019).
- [69] T. D. Jacobs and R. W. Carpick, Nanoscale wear as a stress-assisted chemical reaction, *Nat. Nanotechnol.* **8**, 108 (2013).
- [70] Y. Liu and I. Szlufarska, Chemical Origins of Frictional Aging, *Phys. Rev. Lett.* **109**, 186102 (2012).
- [71] R. Carpick, R. Bernal, P. Chen, J. Schall, J. Harrison, and Y. Jeng, Influence of chemical bonding on the variability of diamond-like carbon nanoscale adhesion: An *in-situ* TEM/nanoindentation and molecular dynamics study, *Microsc. Microanal.* **24**, 1822 (2018).
- [72] T. A. Burgo, T. R. Ducati, K. R. Francisco, K. J. Clinckspoor, F. Galembeck, and S. E. Galembeck, Triboelectricity: Macroscopic charge patterns formed by self-arraying ions on polymer surfaces, *Langmuir* **28**, 7407 (2012).
- [73] R. F. Gouveia, C. A. Costa, and F. Galembeck, Water vapor adsorption effect on silica surface electrostatic patterning, *J. Phys. Chem. C* **112**, 17193 (2008).
- [74] T. R. Ducati, L. H. Simões, and F. Galembeck, Charge partitioning at gas–solid interfaces: Humidity causes electricity buildup on metals, *Langmuir* **26**, 13763 (2010).
- [75] K. S. Moreira, D. Lermen, Y. A. S. da Campo, L. O. Ferreira, and T. A. Burgo, Spontaneous mosaics of charge formed by liquid evaporation, *Adv. Mater. Interfaces* **7**, 2000884 (2020).
- [76] C. Mizzi, A. Lin, and L. Marks, Does Flexoelectricity Drive Triboelectricity?, *Phys. Rev. Lett.* **123**, 116103 (2019).
- [77] C. Mizzi and L. Marks, When flexoelectricity drives triboelectricity, *Nano Lett.* **22**, 3939 (2022).
- [78] K. Olson, C. Mizzi, and L. Marks, Band bending and ratcheting explain triboelectricity in a flexoelectric contact diode, *Nano Lett.* **22**, 3914 (2022).
- [79] E. C. Shin, J. H. Ko, H. K. Lyeo, and Y. H. Kim, Derivation of a governing rule in triboelectric charging and series from thermoelectricity, *Phys. Rev. Res.* **4**, 023131 (2022).
- [80] Z. L. Wang, Triboelectric nanogenerators as new energy technology for self-powered systems and as active mechanical and chemical sensors, *ACS Nano* **7**, 9533 (2013).
- [81] F. Tielens, C. Gervais, J. F. Lambert, F. Mauri, and D. Costa, *Ab initio* study of the hydroxylated surface of amorphous silica: A representative model, *Chem. Mater.* **20**, 3336 (2008).
- [82] H. Jabraoui, T. Charpentier, S. Gin, J.-M. Delaye, and R. Pollet, Atomic insights into the events governing the borosilicate glass–water interface, *J. Phys. Chem. C* **125**, 7919 (2021).
- [83] F. P. Bowden and D. Tabor, The friction and lubrication of solids, *Am. J. Phys.* **19**, 428 (1951).
- [84] I. Singer and H. Pollock, *Fundamentals of Friction: Macroscopic and Microscopic Processes* (Springer Science & Business Media, Braunschweig, 1991), Vol. 220.
- [85] L.-T. Li, X.-M. Liang, Y.-Z. Xing, D. Yan, and G.-F. Wang, Measurement of real contact, *J. Tribol.* **143**, 071501 (2021).
- [86] P. Piotrowski, R. Cannara, G. Gao, J. Urban, R. Carpick, and J. Harrison, Atomistic factors governing adhesion between diamond, amorphous carbon and model diamond nano-composite surfaces, *J. Adhes. Sci. Technol.* **24**, 2471 (2010).
- [87] F. P. Bowden and D. Tabor, The area of contact between stationary and moving surfaces, *Proc. R. Soc. A* **169**, 391 (1939).
- [88] N. Gosvami, B. J. F. Mangolini, A. Konicek, D. Yablon, and R. Carpick, Mechanisms of antiwear tribofilm growth revealed *in situ* by single-asperity sliding contacts, *Science* **348**, 102 (2015).
- [89] M. Kalin, Influence of flash temperatures on the tribological behaviour in low-speed sliding: A review, *Mater. Sci. Eng.* **374**, 390 (2004).
- [90] X. Han, K. Asare-Yeboah, Z. He, C. Jiang, and S. Bi, Mosaic charge distribution-based sliding and pressing triboelectrification under wavy configuration, *J. Phys. Chem. Lett.* **14**, 2509 (2023).
- [91] G. Livia, P. V. Susho, G. Pacchioni, and A. L. Shluger, Electron Trapping at Point Defects on Hydroxylated Silica Surfaces, *Phys. Rev. Lett.* **99**, 136801 (2007).
- [92] A.-M. El-Sayed, M. B. Watkins, V. V. Afanas'ev, and A. L. Shluger, Nature of intrinsic and extrinsic electron trapping in SiO_2 , *Phys. Rev. B* **89**, 125201 (2014).
- [93] F. U. P. Musso, X. Solans-Monfort, and M. Sodupe, Periodic DFT study of radical species on crystalline silica surfaces, *J. Phys. Chem. C* **114**, 16430 (2010).
- [94] G. Pacchioni, L. Skuja, and D. L. Griscom, *Defects in SiO_2 and Related Dielectrics: Science and Technology* (Springer Science & Business Media, 2012).
- [95] E. Bussmann and C. Williams, Single-electron tunneling force spectroscopy of an individual electronic state in a nonconducting surface, *Appl. Phys. Lett.* **88**, 263108 (2006).
- [96] M. M. Smedskjaer, J. C. Mauro, R. E. Youngman, C. L. Hogue, M. Potuzak, and Y. Yue, Topological principles of borosilicate glass chemistry, *J. Phys. Chem. B* **115**, 12930 (2011).